eJSE International

Electronic Journal of Structural Engineering 19(1) 2019

Shear Strengthening of RC Beams Using NSM GFRP Bars or CFRP U-Wrap Sheets

E.Y. Sayed-Ahmed , M.N. Abou-Zeid
Professor, Construction Engineering Dept., the American University in Cairo, Egypt

Helen S. Ghali, Haidy S. Ghali
Dept. of Construction Eng., the American University in Cairo, Egypt

R.M. Armanious
Felobater for Import and Export, Egypt

ABSTRACT: Fiber-reinforced polymers (FRPs) have been in view for the past three decades due to their high strength-to-weight ratio and resistance to corrosion. They are widely used as sheets, externally adhered to reinforced concrete (RC) beams to be strengthened in shear. Although this technique is common, FRP sheets are exposed during their service life to environmental factors. As such, near-surface mounted (NSM) FRP bars may be more favored in shear strengthening of RC beams. Thus, this work experimentally investigates the performance of RC beams strengthened in shear using NSM FRP bars. The experimental results are compared to provisions of ACI 440.2-08 for FRP laminates and to design procedures proposed by De Lorenzis and Nanni (2001) and Dias and Barros (2010) for NSM bars. The current investigation reveals that ACI 440.2-08 overestimate the shear capacity of strengthened beams for widely spaced FRP laminate; thus, an upper limit on the spacing between the sheets should be included in the current provisions. On the other hand, De Lorenzis and Nanni model correctly predicts the capacity of beams strengthened in shear using NSM bar; however, this model still needs a limit on the minimum spacing between the NSM bars.

Keyword: carbon fiber reinforced polymers; FRP debonding; CFRP sheets; GFRP bars, near surface mounted bars; shear strengthening.

1 INTRODUCTION

The need for repairing damaged structural elements and strengthening existing structures has recently become more urgent. Strengthening existing structures started by using steel plates, which were mechanically adhered to the structural elements. However, due to the high own weight of the steel plates, this method deemed to be uneconomic, inefficient and time-consuming. Later, fiber-reinforced polymers (FRPs) were introduced: they are composites of fibers (glass, carbon or aramid) and matrix (epoxy-based resin) that bonds the fibers together. FRPs proved to be extremely efficient for repair and strengthening applications due to their high strength-to-weight ratio and resistance to corroding agents compared to traditional steel plates (Chaallal et al. 1998, Grace 1999, Sayed-Ahmed et al. 2004, Hosny et al. 2006).

Application of FRPs has started by externally bonding FRP laminates, e.g. carbon fiber reinforced polymer (CFRP) sheets/strips, to flexural RC structural elements (beams and slabs) at their weak sections in order to boost the RC elements' capacity. However, premature laminates debonding (Chen and Teng 2003, Sayed-Ahmed et al. 2009, Bakay et al. 2009) dominates failure leading to mobilizing low percentage of the FRP laminates maximum strain. When used in shear strengthening of RC beams, premature debonding from the concrete is also expected to take place (Khalifa et al. 1998, Chen and Teng 2003, Petrone and Monti 2014). Many researchers investigated this shear strengthening technique for RC beams (Alexander and Cheng 1996, Araki et al. 1997, Fanning and Kelly 1999, Hutchinson and Rizkalla 1999, Kachlakev and Barnes 1999, Khalifa 1999, Khalif et al. 1999, Triantafillou and Antonopoulos 2000, Khallifa and Nanni 2000, Teng et al. 2000, Teng et al. 2002, Akroush et al. 2017).

More recently, near-surface mounted (NSM) reinforcement has attracted the attention of researchers and designers (De Lorenzis and Nanni 2001, Nanni et al, 2004, Sena-Cruz and Barros 2004, El-Hacha and Riskalla 2004, Barros and Dias 2006, Rizzo and De Lorenzis 2009, Dias and Barros 2010). This

method involves cutting grooves in the designated RC member, and then FRP bars or laminates are placed in these grooves and bonded to the concrete using epoxy resin. This technique has proven to be more effective than using externally bonded FRP laminates because NSM reinforcement has better bonding properties with concrete, and thus less vulnerable to the premature debonding failure. NSM strengthening technique is also more durable since reinforcement is protected by the concrete and epoxy cover, unlike the externally bonded FRP laminates. Furthermore, the NSM strengthening technique requires less surface preparation and installation time. Despite that, research related to using NSM technique in shear strengthening of RC beams is still lagging behind. For example, among the currently available research on the capacity of RC beams strengthened in shear using NSM FRP bars or laminates is the one performed by De Lorenzis and Nanni (2001). They tested twelve RC T-beams strengthened in shear using NSM FRP bars to investigate the effect of various parameters on the beam's shear capacity such as the effect of anchoring the NSM bars in the beams flange, the NSM bars' spacing and inclination, and the presence of shear reinforcement. Test results showed that decreasing the spacing from 7 in (178 mm) to 5 in (127 mm) increased the shear capacity by 7.5%. Furthermore, changing the NSM bar inclination from 90° to 45°, increased the shear capacity by 134.5%. They also found out that anchoring the NSM bars into the beam's flange prevented debonding failure and decreases the shear reinforcement while increased the shear capacity of the beams. Using the experimental investigation results, they developed a design equation to calculate the shear strength of an NSM strengthened RC beam which is by

$$V_f = \tau_{bond} \left(2 \pi d_b\right) L_{tot} \quad (1)$$

where V_f is the shear contribution of NSM FRP bars, d_b is bar diameter and L_{tot} is the total length intercepted by a shear crack (will be explained later). This equation was verified against their experimental work showing an average variation of 32%.

In another research, Dias and Barros (2010) investigated the shear strengthening of RC beams by comparing the usage of NSM CFRP laminates and CFRP U-wrap sheets. They drew similar conclusions to that of Lorenzis and Nanni [22] regarding the effect of NSM laminates' spacing and inclination. They also compared the externally bonded FRP laminate technique vis-à-vis the NSM bar one and they concluded that NSM bar strengthening technique is more effective in terms of the ultimate load and the post-cracking behavior showing a stiffer load-deflection performance. They compared their experimental results with the theoretical equations available for both techniques. Regarding the NSM strengthening technique, they compared their results to De Lorenzis and Nanni (2001) model; the latter was conservative showing 1.04 to 3.9 (with an average of 1.91) capacity folds of the experimental values. For the externally bonded FRP laminate technique, the experimental results were compared to ACI 440.2-08 and *fib* provisions, which were also found to be conservative.

Thus, in light of the above and the lack of research results in the area of shear strengthening RC beams using NSM reinforcement, the objective of the current investigation is to experimentally scrutinize the performance of the shear strengthening techniques for RC beams using NSM GFRP bars and U-wrap CFRP laminate. The results of the experimental investigation are then used to validate the currently used design equations for each technique.

2 THE EXPERIMENTAL INVESTIGATION

An experimental program was designed to investigate two different shear strengthening techniques for RC beams: near-surface mounted (NSM) strengthening using glass fiber reinforced polymer (GFRP) bars and externally bonded laminate strengthening using the unidirectional U-wrap CFRP sheets.

The program encompassed fourteen RC beams with a length of 1.8 m and a testing span of 1.5 m (Figure 1). The beam's cross-section was designed as a T-section to avoid concrete crushing in the top concrete fibers. The shear span is 0.75 m; that is 2.6 times the effective depth, thus arching effect is negligible (Collins and Mitchell 1997).

The beam, shown in Figure 1, has two sides A and B: Side A is shear deficient where shear strengthening will be applied and Side B is adequately shear-reinforced to ensure shear failure at side A. The shear reinforcement of sides A and B consisted of single loop stirrups with a diameter of 8 mm spaced at 220 mm ($\rho_{stirrups}$ = 0.15%) and a diameter of 10 mm spaced at 75 mm ($\rho_{stirrups}$ = 0.70%), respectively. The stirrups, plain coil grade 280, has a yield and ultimate strength of 280 and 450 MPa, respectively. Flexure reinforcement is composed of 2 no. 10 + 2 no. 16 deformed bars top reinforcement and 4 no. 25 deformed bars (arranged on two layers) bottom reinforcement. Both top and bot-

tom reinforcement have a yield and ultimate strength of 360 and 520 MPa, respectively. Shear and flexural reinforcement were designed to ensure shear failure in the strengthened side (Side A). The beams were tested in 3-point loading as shown in Figure 2.

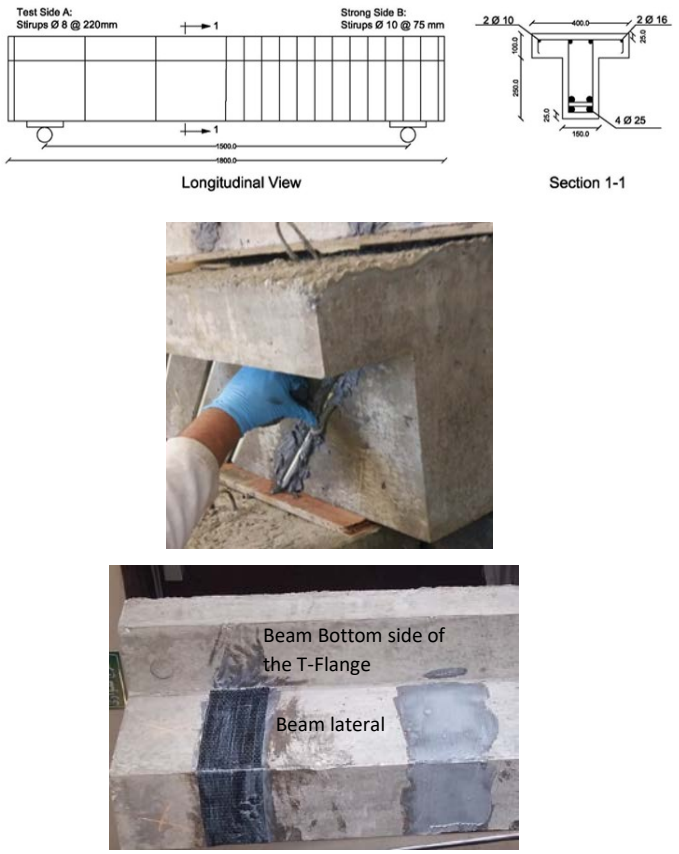

Figure 1 Details of the tested beams.

The fourteen tested beams were divided into 10 different sets as listed in Table 1 and shown in Figure 3. Set 1, the control set used for comparison, is composed of two beams. Sets 2 to 4, each contains two beams, were strengthened using NSM GFRP 12 mm diameter bars with three different spacing: 540 mm, 270 mm and 180 mm. Sets 5 to 10 each has one beam and was strengthened with one layer of CFRP U-wrap 0.12 mm thick laminates in six different configurations.

All beams are assigned ID codes, which start with a letter B, indicative for Beam, followed by two numbers: the first refers to the set number and the second refers to the beam number. The second designation accounts for the adopted shear strengthening system: NSM stands for near-surface mounted GFRP bars and UW stands for externally bonded CFRP U-wrap system. The third designation refers to the spacing used in case of the NSM system or the width of the U-wrap sheets. The last designation that only exists for U-wrap sets refers to the number of U-wrap sheets used in each beam.

The concrete in its fresh state had a slump of 16.5 mm. The 7-day compressive strength of a standard cube (150×150×150 mm) was 40.3 MPa, and the 14-day compressive strength of two cubes was 51 MPa (an average of 49.0 MPa and 52.8 MPa). The 28-day compressive strength was 53 MPa.

The GFRP bars used in the current investigation has Young's Modulus and ultimate tensile strength of 60 GPa and 1350 MPa, respectively. On the other hand, Sika C-300 CFRP sheets have Young's modulus of 242 MPa, elongation at failure of 0.17 mm and ultimate strain of 0.0155. MasterBrace 4000 epoxy was used to bond the NSM bars while SikaDur 300 epoxy was used to bond the CFRP sheets.

A typical example for installation of the NSM GFRP bars and bonding the U-wrap CFRP sheets is shown in Figure 1. For beams strengthened with NSM bars, pre-cut grooves were created in the formwork by wooden strips having a depth of 18 mm (1.5 times the 12 mm diameter of the GFRP bar) with a width of 20 mm and a length of 350 mm. After 28 days of curing, the formwork and the wooden strips were removed. Epoxy was mixed according to the manufacturer's recommended procedures and the grooves were filled with epoxy while the GFRP bar inserted in these grooves. Any residual epoxy was removed and, then, the surface was finished. The epoxy was left for two weeks to gain its strength before testing the beams. The NSM GFRP bars were placed at an angle of 45^o with the beam axis since this is the most effective inclination as compared to the 90^o and 60^o angels (De Lorenzis and Nanni 2001, Nanni et al. 2004, Sena-Cruz and Barros 2004, El-Hacha and Riskalla 2004, Barros and Dias 2006, Rizzo and De Lorenzis 2009, Dias and Barros 2010).

For CFRP strengthened beams, surfaces in the vicinity of the region where the sheets to be bonded was cleaned with an air compressor and the beam's edges were round using a saw cutter. The sheets were cut to the intended widths and the epoxy was mixed according to the manufacturer's recommended procedures. Using a sponge hard roller an initial epoxy layer was applied on the said region and the sheets were then applied, followed by a final epoxy layer to release the trapped air.

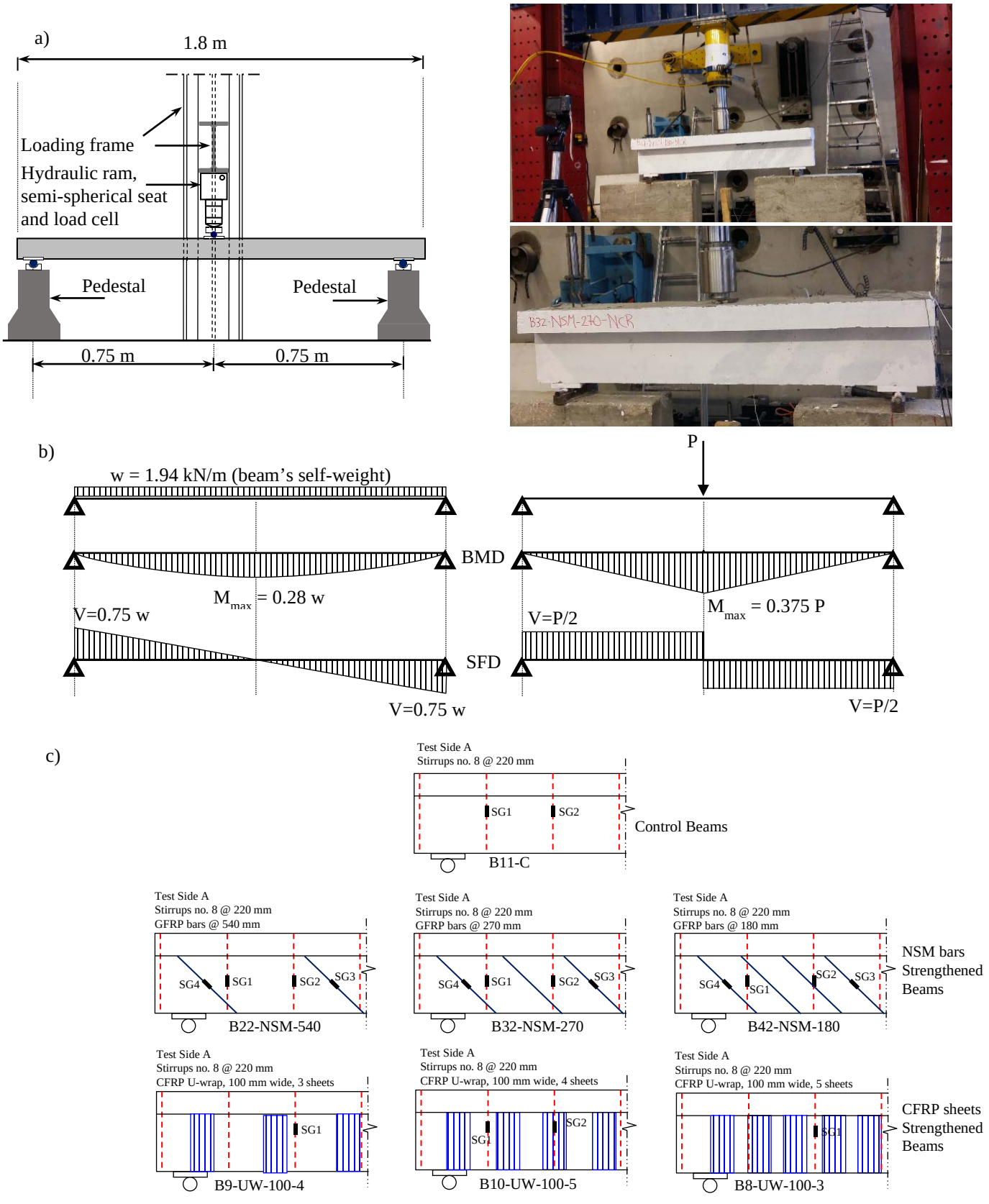

Figure 2. a) Test set-up, b) Bending moment and shear force, c) Strain gauges

Three-point bending test was conducted on all beams with a load cell and an LVDT was placed in the mid-span of the beam in order to monitor the load-deflection behavior. Strain gauges were attached to the steel stirrups on the beam's shear-defected side and on the GFRP bars in order to monitor the change in the strain with the applied load. The number and locations of the strain gauges are shown in Table 2 and Figure 2c.

The experimental program configuration described above allows scrutinizing the effect of changing the spacing between the NSM GFRP bars.

The investigation also compares the effectiveness of using U-wrap CFRP sheets as a shear strengthening technique placed in different configurations and compare them to the NSM bars strengthening technique. Given that failure occurs mostly by deboning in the two investigated strengthening techniques, the difference in materials (GFRP bars versus CFRP sheets) will not be of a concern as beams would have failed before both materials reach their ultimate strength.

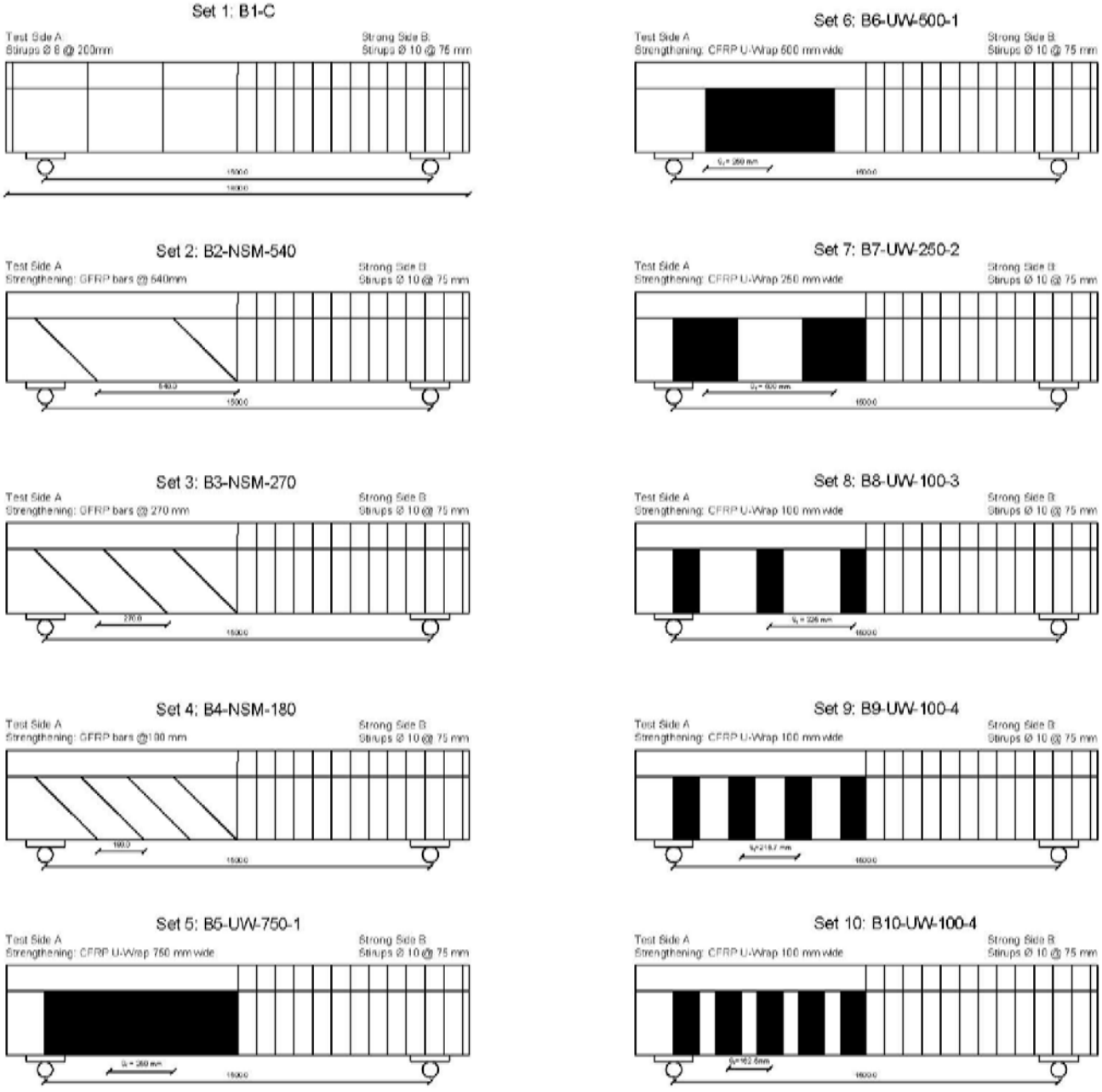

Figure 3. Configurations of the NSM GFRP bars and the U-wrap CFRP laminates.

3 RESULTS OF THE EXPERIMENTAL INVESTIGATION

Table 3 summarizes the results of all the tested beams. In this table, Columns 1 and 2 display the set number and the beam's ID, respectively. Column 3 shows the FRP reinforcement ratio ρ_{FRP} for both strengthening techniques. Columns 4 and 7 show the initial cracking load (the load at the first appearance of the shear crack) and the ultimate failure load, respectively. The averages of the cracking loads (for NSM strengthened beams) and failure loads (for all beams) are shown in the 5th and 8th columns, respectively.

Columns 6 and 9 of Table 3 show the FRP contributions to the beam's cracking and ultimate loads ($P_{cr\text{-}f}$ and $P_{u\text{-}f}$), respectively. This contribution was calculated as the difference between the control beam's cracking or failure loads and those for the

strengthened beam. The percentage increases in the cracking and failure loads above that of the control beam were computed and listed in the last two columns of Table 3, while the 10th column shows the ratio of the ultimate to cracking load of each set.

Table 1. Details of the tested beams of the experimental program.

Set	Beam ID	Strengthening technique	GFRP bars or CFRP sheets	Spacing mm	Angle deg.	Reinf. ratio ρ_{FRP}
1	B11-C	--	--	-	-	
	B12-C	--	--	-	-	
2	B21-NSM-540	NSM-GFRP	2 Bars at 540 mm	540	45	0.28%
	B22-NSM-540	NSM-GFRP	2 Bars at 540 mm	540	45	0.28%
3	B31-NSM-270	NSM-GFRP	3 Bars at 270 mm	270	45	0.56%
	B32-NSM-270	NSM-GFRP	3 Bars at 270 mm	270	45	0.56%
4	B41-NSM-180	NSM-GFRP	4 Bars at 180 mm	180	45	0.84%
	B42-NSM-180	NSM-GFRP	4 Bars at 180 mm	180	45	0.84%
5	B5-UW-750-1	CFRP U-wrap	1 sheet - width 750 mm	250	90	0.48%
6	B6-UW-500-1	CFRP U-wrap	1 sheet - width 500 mm	250	90	0.16%
7	B7-UW-250-2	CFRP U-wrap	2 sheets - width 250 mm	250	90	0.08%
8	B8-UW-100-3	CFRP U-wrap	3 sheets - width 100 mm	325	90	0.05%
9	B9-UW-100-4	CFRP U-wrap	4 sheets - width 100 mm	216.7	90	0.07%
10	B10-UW-100-5	CFRP U-wrap	5 sheets - width 100 mm	162.5	90	0.098%

Table 2. Strain gauges locations and configuration.

Set	Beam ID	Strain gauges' location and number		Strain gauges configuration (Figure 2c)
1	B11-C	Stirrups	2 gauges	1st and 2nd stirrups from the support.
2	B22-NSM-540	Stirrups	2 gauges	1st and 2nd stirrups from the support.
		GFRP-NSM	2 gauges	1st and 2nd GFRP bars from the support.
3	B32-NSM-270	Stirrups	2 gauges	1st and 2nd stirrups from the support.
		GFRP-NSM	2 gauges	1st and 3rd GFRP bars from the support.
4	B42-NSM-180	Stirrups	2 gauges	1st and 2nd stirrups from the support.
		GFRP-NSM	2 gauges	1st and 4th GFRP bars from the support.
8	B8-UW-100-3	Stirrups	1 gauge	2nd stirrup from the support.
		CFRP-U-wrap	-----	----
9	B9-UW-100-4	Stirrups	2 gauges	1st and 2nd stirrups from the support.
		CFRP-U-wrap	-----	----
10	B10-UW-100-5	Stirrups	1 gauge	2nd stirrup from the support.
		CFRP-U-wrap	-----	----

Table 3. Results of the experimental investigation for all beams.

Set	Beam ID	Reinf. ratio ρ_{FRP}%	Cracking load P_{cr} (kN)			Ultimate load P_u (kN)			P_u/P_{cr}	% increase in	
			Value	Av.	$P_{cr\text{-}f}$	Value	Av.	$P_{u\text{-}f}$		P_{cr}	P_u
1	B11-C	0	225.6	220.7	0	354.2	359.6	0	1.63	--	--
	B12-C		215.8			365.0					
2	B21-NSM-540	0.28	225.6	245.3	24.6	378.6	386.9	27.3	1.58	11.1%	7.6%
	B22-NSM-540		264.9			395.2					
3	B31-NSM-270	0.56	461.1	451.3	230.6	484.9	478.0	110.4	1.06	104.5%	32.9%
	B32-NSM-270		441.5			471.0					
4	B41-NSM-180	0.84	500.3	501.4	280.7	510.1	508.7	149.1	1.01	127.2%	41.4%
	B42-NSM-180		502.4			507.2					
5	B5-UW-750-1	0.48	--	--	--	472.7	472.7	113.1	--	--	31.5%
6	B6-UW-500-1	0.16	--	--	--	469.4	469.4	109.8	--	--	30.5%
7	B7-UW-250-2	0.08	--	--	--	387.4	387.4	27.8	--	--	7.7%
8	B8-UW-100-3	0.05	--	--	--	463.8	463.8	104.2	--	--	29.0%
9	B9-UW-100-4	0.07	--	--	--	416.2	416.2	56.6	--	--	15.8%
10	B10-UW-100-5	0.10	--	--	--	442.8	442.8	83.2	--	--	23.1%

Furthermore, Figure 4 shows the load-deflection relation for the strengthened beams compared to the control beam (Beam B12-C) which is chosen as a reference for comparison.

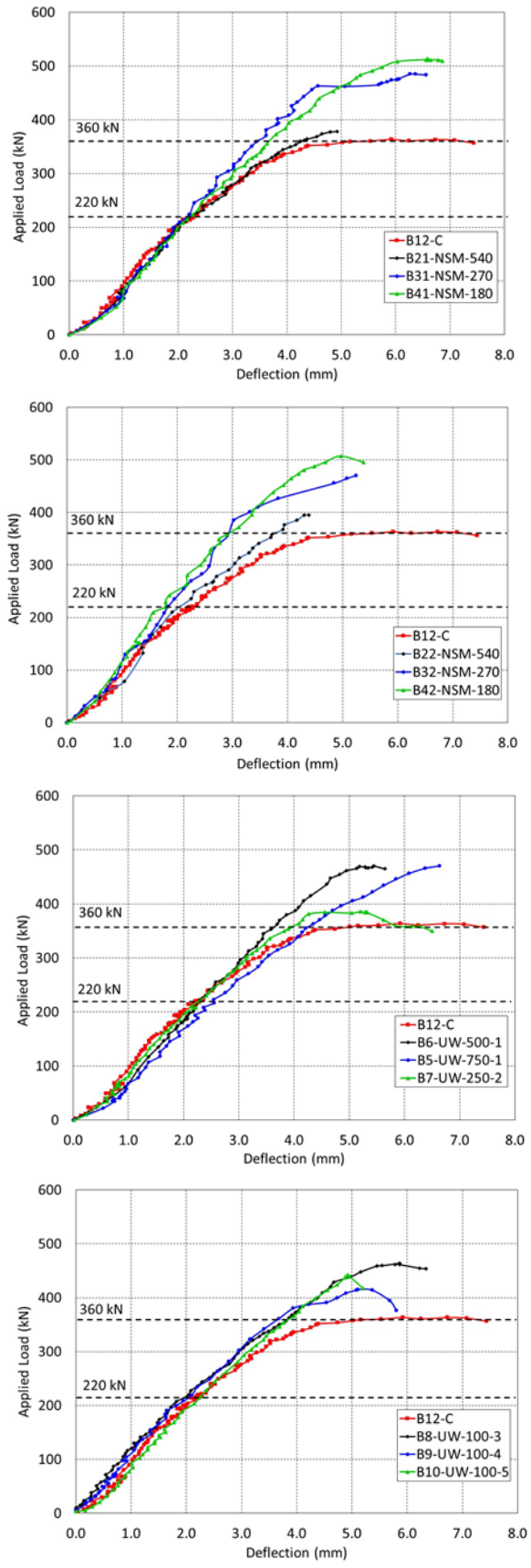

Figure 4. Load-deflection behavior for the tested beams.

The experimental results listed in Table 3 and plotted in Figure 4 reveal that both the NSM GFRP bars and the U-wrap CFRP sheets strengthening techniques increase the cracking and the failure loads of the strengthened beams as expected. For the control beams (Set 1), the average cracking load was 220 kN while the average failure load was at 360 kN (P_u/P_{cr} = 1.63).

For NSM beams of Sets 2, 3 and 4, the increase in the cracking load was 11%, 104%, and 127%, respectively. Regarding the failure load, the recorded increase in the shear capacity of these beam sets was 7.6%, 33%, and 41%, respectively. From these data, it is evident that the percentage increase in the cracking load is consistently higher than that of the failure load; failure of NSM strengthened beams occurred at a load value close to the cracking load. In contrary to the control beam where failure load was almost 1.6 times the cracking load, the NSM strengthened beam sets, showed failure loads which are 1.58, 1.06, and 1.01 the cracking loads for bar spacing of 540 mm, 270 mm and 180 mm, respectively (Sets 2, 3 and 4). These results illustrate the favored crack-bridging effect of the NSM bars; the bars crossing the initial shear crack prevented it from further propagation after the aggregate interlock is lost at about 220 kN (the ultimate load of the control set). As seen in Figure 4, at 220 kN, after the initiation of the 1st shear crack, NSM Sets 3 and 4 stiffness does not drop as seen for the control beam, meaning that the strengthened beams exhibit a stiffer behavior than that of the control beam.

It is worth mentioning that the increase in the cracking load or the failure load is not proportional to the increase in the FRP shear reinforcement ratio ρ_{FRP} of the NSM strengthened beams. For these beams, Table 3 show that the increase in the NSM shear reinforcement ratio from 0.28% to 0.84% (i.e. 0.56%) increases the cracking load from 11% to 127% (i.e. 116%) and the failure load from 7.6% to 41.4% (i.e. 33.8%) revealing the favorable effect of the crack-bridging behavior explained above. Similar behavior is also evident for CFRP U-wrap laminates strengthened beams (Table 3).

4 FAILURE MODES

4.1 *Control beams*

In Set 1 (control beams), the initial shear crack shown in Figure 5a was observed during testing at an average load of 220.7 kN. The beams were loaded to failure, which occurred at an average load of 359.6 kN (P_u/P_{cr} = 1.63).

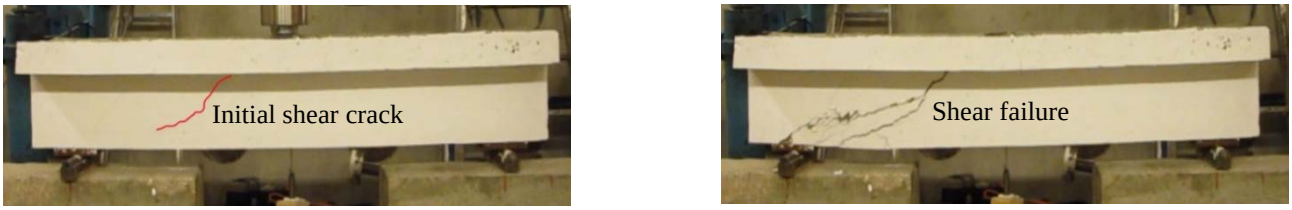

a) Control beams (Set 1)

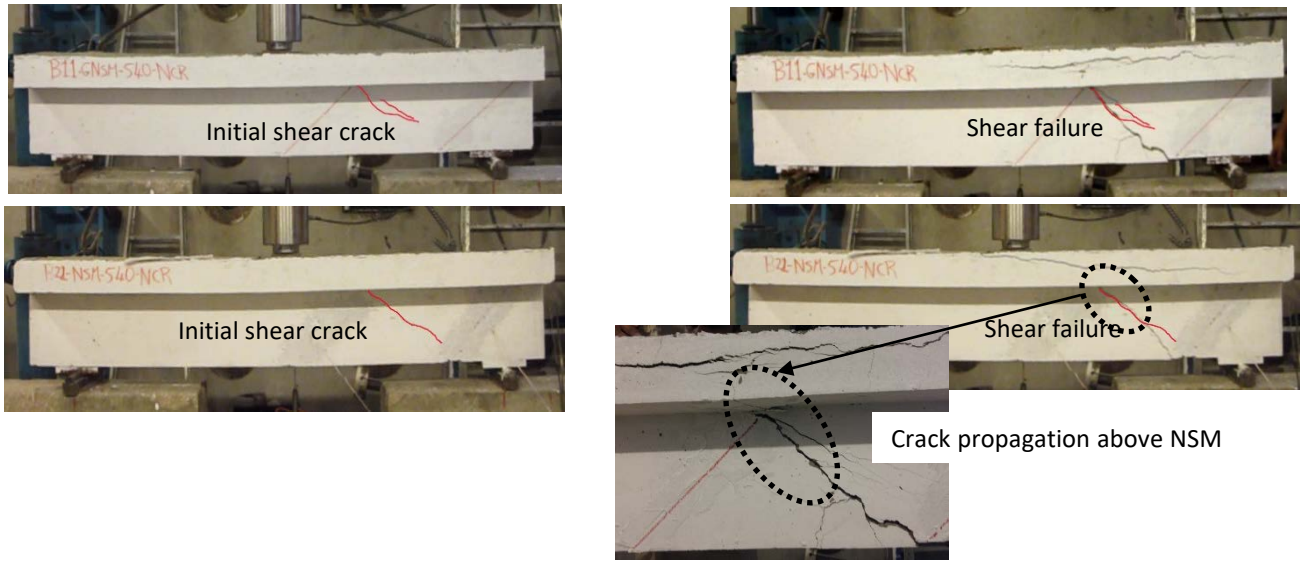

b) NSM strengthened beams with 540 mm bar spacing (Set 2)

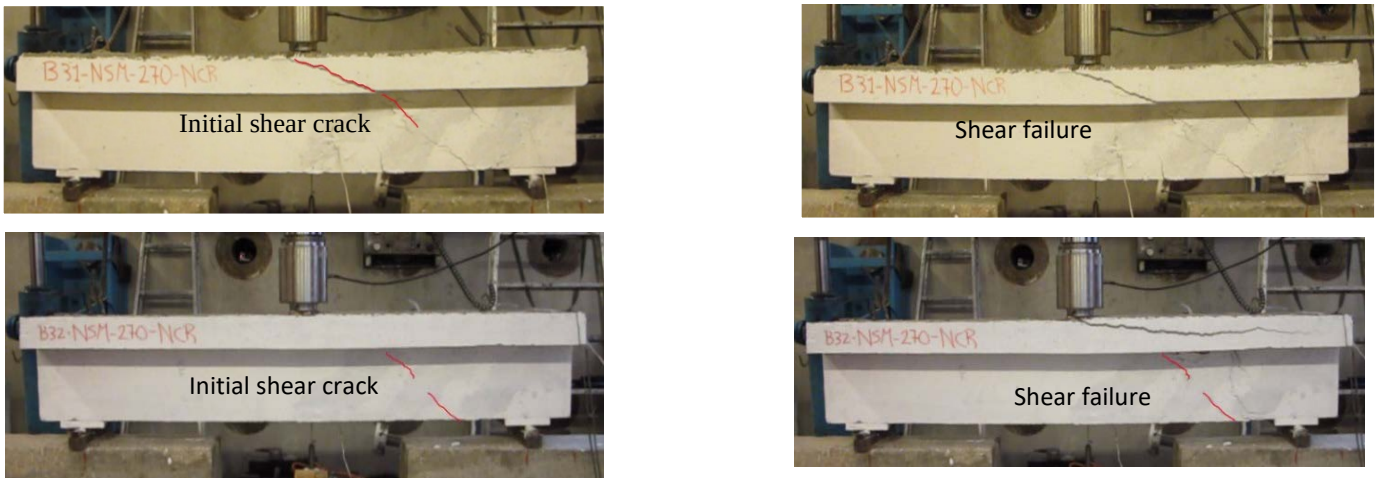

c) NSM strengthened beams with 270 mm bar spacing (Set 3)

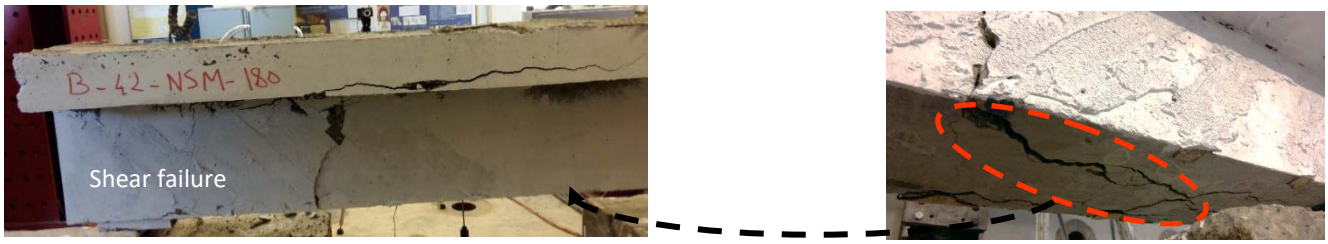

d) NSM strengthened beams with 180 mm bar spacing (Set 4)

Figure 5. Crack initiation and failure of control and NSM strengthened beams

The major shear crack causing failure propagated from the location of the applied load until reaching the support at failure.

The readings of strain gauges located on the 2nd and 3rd stirrups (Table 2 and Figure 2c) are plotted in Figure 6. As seen in this figure, the strain gauge SG-

2 reading is higher than that recorded by SG-1 since it is closer to the applied load, therefore depicts higher strain. Accordingly, the initial strain reading of SG-2 and SG-1 occurred at loading 145 kN and 161 kN respectively; indicating loss of concrete shear resistance. Internally, the aggregate interlock was lost at 145 kN and 161 kN and the initial crack was visually observed at 220.7 kN.

4.2 *Beams strengthened with NSM GFRP bars*

For the two beams of Set 2 (B2-NSM-540), the first shear crack (Figure 5b), were observed at 225.6 kN and 264.9 kN. The initial shear crack propagated from the load at approximately an angle of 45^{o} and passed through the top of the first NSM bar near the load location (Figure 5b). Then, the crack propagated between the two GFRP bars and the beams failed at an average load of 386.9 kN (P_u/P_{cr} = 1.58), which is approximately the same load as that of the control beams.

In this set (B2-NSM-540), the NSM strengthening was not effective because the crack did not intersect any of the NSM GFRP bars; it rather propagated in the 540 mm spacing between the bars. The readings of the strain gauge mounted on the steel stirrups and the GFRP bars (Table 2 and Figure 2c) are plotted in Figure 6. The steel strain gauge nearest to the crack propagation from the loading cell, namely SG-2, recorded the highest strain values, while stain gauge SG-1 (further from the load) recorded lower values. SG-2 started to record elongation indicating an initial crack at 222.5 kN, which is a close value to the visually observed crack. SG-1 almost did not record any elongation, except for a slight strain at failure when the crack propagated to the support, because the crack did not pass across this stirrup as it escaped between the two NSM bars and did not even reach the 2nd stirrup. Strain gauge SG3 mounted on the GFRP bars (Table 2 and Figure 2c) was the first to record a reading and had higher strain values than that of SG-4 because it was the nearest to the crack initiation and propagation.

The GFRP bars' strain gauges have recorded values from the start of loading; on the contrary to the steel stirrups strain gauges which recorded values only at loss of the concrete shear resistance that was encountered just before cracking. Therefore, although the 540 mm spacing is not efficient in increasing the beam's capacity, it was efficient in delaying the crack initiation by almost 58% of the control beam's cracking load.

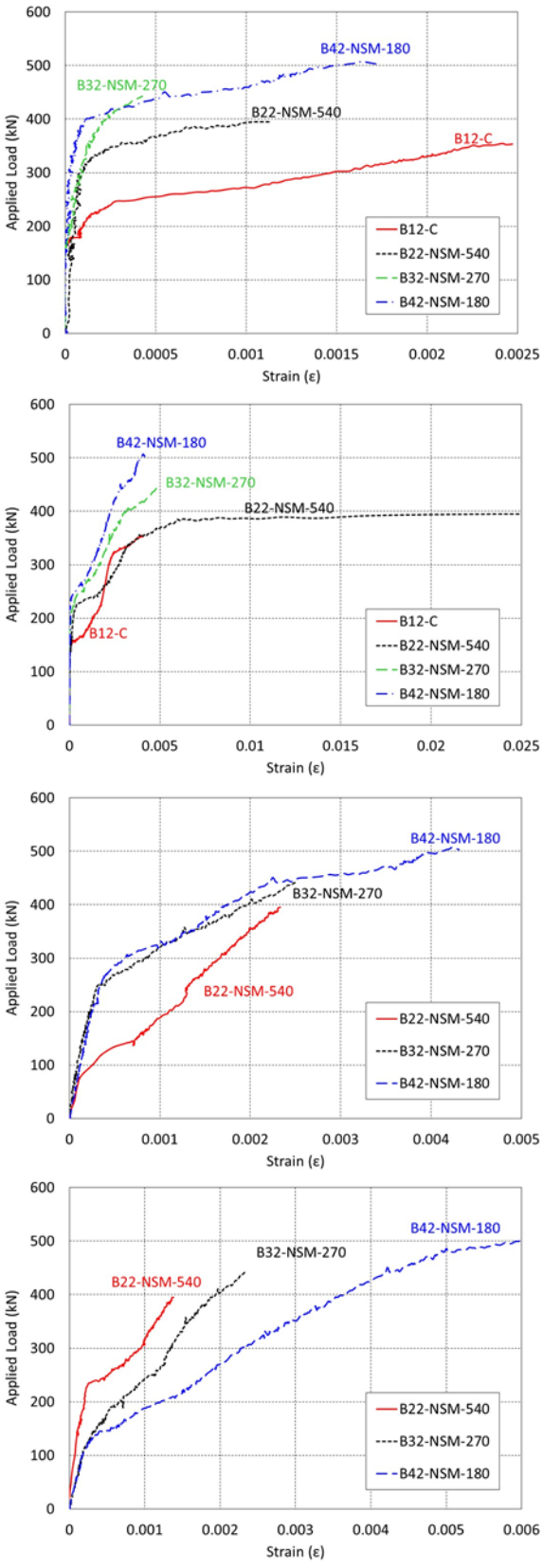

Figure 6. Strain gauge readings for control and NSM beams.

For the two beams of Set 3 (B3-NSM-270), the initial crack appeared at an average load of 451.3 kN (Figure 5c) and shear failure occurred at an average load of 478.0 kN (P_u/P_{cr} = 1.06). Cracking started from the loading point in the mid-span of the beam

and passed through the flange but did not interfere with the 1st NSM GFRP bar. Then, the crack reached the 2nd GFRP bar where this bar prevented the shear crack from further propagation; the shear crack was arrested and stopped at the location of this bar. Another shear crack initiated near the support at the tip of the NSM bar then propagated until reaching the 2nd NSM bar but was stopped too. Later, the beams failed due to the propagation of these two shear cracks. The arrest of the 1st shear crack and the initiation of the 2nd crack was indeed due to the presence of three NSM GFRP bars. The strain gauge readings behavior were similar to those observed for NSM bars spaced at 540 mm. The strain gauge on the NSM bar had recorded values, while the strain gauges on the steel stirrups did not record any values except after 250 kN, meaning that the contribution of the NSM bar to the beam's shear strength occurred prior to the contribution of the steel stirrups.

Beams of Set 4 (B4-NSM-180) with the narrow spacing of 180 mm between the NSM GFRP bars, did not significantly increase the failure load beyond that of Set 3 beams with 270 mm spacing between the GFRP bars. The first shear crack for this set appeared in the non-shear deficient side A at 500.3 kN and 502.4 kN. Before this crack developed to cause failure, another crack propagated from the load location through the flange and passed through the top of the 1st bar near the load. Then, it propagated to the 2nd bar and at the same time, another shear crack started at the tip of the 3rd bar from the support (Figure 5d). Beam failure was encountered due to a crack propagating in the middle of the beam's web (Figure 5d) as the GFRP was only mounted on the two sides of the web and did not cross the beam's soffit. The strain gauge readings were similar to those observed for beams with NSM bars spaced at 540 mm and 270 mm. The strain gauges mounted on the NSM bar had recorded values, while those mounted on the steel stirrups did not record any values except after the load reached 250 kN; one again, the contribution of the NSM bar to the beam's shear strength occurred prior to the contribution of the steel stirrups.

4.3 *Beams strengthened with CFRP sheets*

All beams strengthened with CFRP U-warp sheets encountered failure mainly by debonding of the CFRP sheet at the concrete epoxy interface (Figure 7). The six sets of these beams (Sets 5 to 10) can be classified into two major groups. The first group comprised of Sets 5, 6 and 7 where "wide" CFRP sheets (250 mm wide) were used with different centreline to centreline spacing. On the other hand, the second group (Sets 8, 9 and 10) had "narrow" sheets (100 mm wide) with different centreline to centreline spacing.

For beam B5-UW-750-1 (Set 5), and as an insight about the installation process, the 750 mm spaced sheet was achieved by installing a 500 mm wide CFRP sheet just beside a 250 mm wide one. Debonding failure started between the 500 mm sheet and the 250 mm sheet (Figure 7a), i.e. along the connection line of the two U-wrap sheet, which is the weakest point. Failure load recorded for this beam was 472.7 kN. Beam B6-UW-500-1 (Set 6) failed at a load of 469.4 kN. Debonding of the CFRP sheets occurred in a vertical line parallel to the sheet fibers (Figure 7b) with the inclined shear crack visible under the sheet after debonding. At failure, the beam recorded a maximum mid-span deflection of 5.6 mm (Figure 4). For Beam B7-UW-250-2 (Set 7), failure occurred a load of 387.4 kN. The shear crack (Figure 7c) initiated from the loading point then passed through the 2nd sheet causing debonding at the concrete epoxy interface. At failure, the beam recorded a maximum mid-span deflection of 5.1 mm (Figure 4). For this group (Sets 5, 6 and 7), it is clear that failure load decreases as the spacing between the sheets increases; i.e. less amount of CFRP sheets are used. Last beam (with clear spacing between the sheets of 250 mm) only achieved a 7.7% capacity enhancement compared to the control beam.

The second group of beams with 100 mm wide sheets actually showed an interesting behavior. Debonding mainly occurred to the 2nd sheet from the support with different crack initiation location. For Beam B8-UW-100-3 (Set 8), failure occurred at a load of 463.8 kN. The shear crack (Figure 7d) initiated from the loading point, then passed through the 2nd sheet, and did not interfere with the 3rd one (the sheet furthest from the support) causing debonding at the concrete-epoxy interface of the 2nd sheet as shown in Figure 7d. At failure, the beam recorded a maximum mid-span deflection of 7 mm (Figure 4).

For Beam B9-UW-100-4 (Set 9), failure occurred at a load of 416.2 kN. This beams recorded significantly lower load compared to beams of Sets 8 and 10 and may be considered as an experimental fault due to an early debonding of the sheets. However, debonding of the CFRP sheets followed the same expected pattern where it occurred at the 3rd sheets (Figure 7e). The shear crack initiated from the loading point passed through the 2nd and 3rd sheets, then the crack reached the tip of the 1st sheet (the one nearest to the support). The shear crack did not inter-

fere with the sheet nearest to the support and the loading point, namely the 1st and 4th sheets, respectively. At failure, the beam recorded a maximum mid-span deflection of 6 mm (Figure 4).

For Beam B10-UW-100-5 (Set 10), failure occurred at a load of 442.8 kN. The shear crack initiated from the loading point passed through the 2nd and 3rd sheets from the support (Figure 7f). The shear crack did not interfere with the sheet nearest to the support and the two sheets near the loading point, namely the 1st, 4th, and 5th sheets, respectively. At failure, the beam recorded a maximum mid-span deflection of 6 mm (Figure 4b).

Strain gauges were mounted on the steel stirrups of the beam sets strengthened with CFRP sheets with the configuration shown in Table 2 and Figure 2c; these are B8-UW-100-3, B9-UW-100-4, and B10-UW-100-5. The readings of these gauges are plotted versus the applied load in Figure 8. It is evident from this figure that unlike the behavior encountered for beams with NSM bars, the stirrups strain gauges started recording strains once the first crack is encountered at about 200 kN to 220 kN. This behavior reveals the more favorable strengthening effect of the NSM bars compared to that of the CFRP sheets. Figure 8 also confirms the premature debonding of the CFRP sheets from the beams (e.g. Beam B9-UW-100-4) as evident from the low values of the recorded strains compared to other beams.

a) CFRP sheets strengthened beam B5-UW-750-1 (Set 5)

b) CFRP sheets strengthened beam B6-UW-500-1 (Set 6)

c) CFRP sheets strengthened beam B7-UW-250-2 (Set 7)

d) CFRP sheets strengthened beam B8-UW-100-3 (Set 8)

e) CFRP sheets strengthened beam B9-UW-100-4 (Set 9)

f) CFRP sheets strengthened beam B10-UW-100-5 (Set 10)

Figure 7. Cracking and failure of beams strengthened with CFRP sheets.

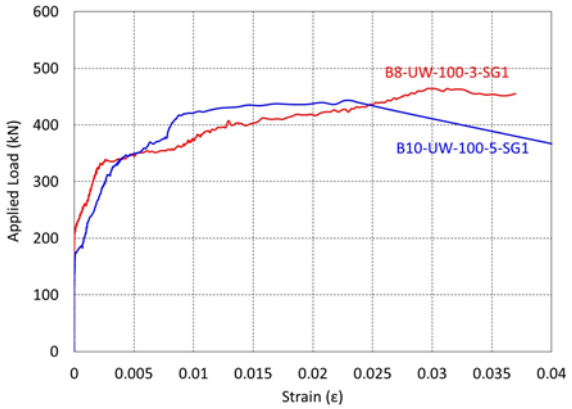

a. Strain Gauge SG1

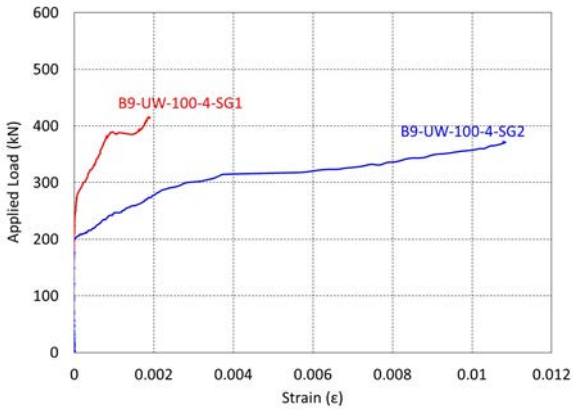

b. Strain Gauge SG1 and SG2

Figure 8. Strain gauge readings for CFRP strengthened beams.

5 NUMERICAL MODELLING OF THE TESTED BEAMS

A nonlinear numerical model based on the finite element method is developed for some of the tested beams via Midas FEA software. The numerical model was merely developed in order to gain more confidence in the results of the experimental program. The model accounts for both material and geometric nonlinearities as well as concrete cracking. Table 4 summarizes the adopted element type, material properties, and cracking/constitutive model for each material.

The slipping behavior that occurs in the concrete-epoxy interface is crucial to obtain realistic results. For that purpose, interface (contact) elements were introduced at these surfaces with normal and shear stiffness moduli 310 GPa/mm and 31 GPa/mm, respectively. Displacement control loading protocol was adopted in the numerical analysis to enhance the convergence requirements during the nonlinear iteration solution module. The boundary conditions were chosen to model a simply supported beam in three-point loading in order to simulate the test set-up. Figure 9 shows a typical finite element mesh adopted for the beams.

Table 4. Numerical model details

Material	Element type used	Material Properties	Cracking and constitutive model
Concrete	Tetrahedron (4 node) solid element	E_c = 15 GPa f_{cu} = 45 MPa f_t = 9.5 MPa	Smeared Crack
Steel	2-node link element	E_s = 200 GPa F_y = 360 MPa	von Mises failure criteria Embedded reinforcement element
Epoxy	Tetrahedron (4 node) element	E_{adh} = 4 GPa	Bond-slip
GFRP	2-node link element	E_f = 60 GPa	Elastic
CFRP	Plate element	E_{11} =15 GPa E_{22} =15 GPa E_{33} =242 GPa	Orthotropic Elastic material

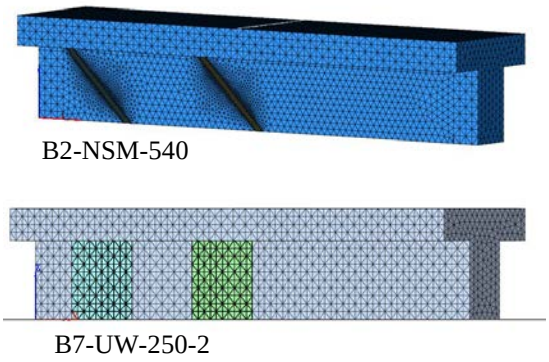

B2-NSM-540

B7-UW-250-2

Figure 9. Example of the FE meshes used to model the beams.

Table 5. Comparison between results of the numerical and experimental analyses.

Beam ID	Ultimate load (kN)		$P_{u\text{-}exp}/P_{u\text{-}FE}$	Max. deflection (mm)		$D_{u\text{-}exp}/D_{u\text{-}FE}$
	$P_{u\text{-}exp}$	$P_{u\text{-}FE}$		$D_{u\text{-}exp}$	$D_{u\text{-}FE}$	
B1-C	359.6	402.8	0.90	-	-	-
B2-NSM-540	386.9	376.6	1.02	5.06	4.13	1.23
B3-NSM-270	478.0	487.6	0.98	7.00	5.33	1.31
B4-NSM-180	508.7	502.3	1.01	7.80	8.13	0.96
B7-UW-250-2	387.4	411.9	0.94	5.10	3.60	1.41

Five beams were numerically analyzed (Table 5): a control beam, three beams with different NSM bar spacing and one beam with U-wrap CFRP sheets. The results of the numerical analysis in terms of ultimate load and maximum mid-span deflection are listed in Table 5 and compared to their counterparts which were experimentally recorded. The results

listed in Table 5 shows that the numerically obtained failure loads well-agree with their experimentally recorded counterparts.

Furthermore, the load-deflection relations numerically obtained are plotted against their experimentally recorded counterparts in Figure 10. The figure reveals an acceptable match between the numerical and the experimental analyses. For example, the load-deflection plots resulting from the finite element analysis and obtained experimentally for beams of Set B4-NSM-180 show a very similar trend in terms of changes in stiffness as the load progresses and the beam approaches failure. However, the numerical model showed an initial stiffer behavior than that of the experimental counterpart.

The principal tensile strain contours resulting from the finite element analysis are plotted in Figure 11 and used to predict the cracking pattern causing failure of the beams. These are also compared to the cracking pattern observed experimentally for the corresponding tested beam.

For the control beam, the numerical model shows that it fails by a major shear crack that develops from the point of load application and propagates towards the support causing failure (Figure 11a); this also well-agree with the experimental observation for this beam. For Beam B2-NSM-540 (Figure 11b), the numerical analysis shows that failure occurs due to a major diagonal shear crack that is confined between the two NSM GFRP bars; similar to what have been experimentally recorded. The model also shows that there are no flexural cracks nor shear cracks on the unstrengthened side of the beam.

It is also evident from Figure 11c that for Beam B4-NSM-180, the numerical model predicted a diagonal shear crack between the two NSM GFRP bars. This crack escapes to the bottom of the beam's web and propagates above the internal NSM bar under the beam flange. The model also predicts minor flexure cracking at the beam's mid-span. Figure 11c shows the stresses developed in both steel stirrups and beam's reinforcement; both of them reaching the yield value of the steel at failure. This behavior agrees with the steel stirrups strain recorded experimentally via strain gauge SG2 (Table 2 and Figure 2c) which is previously plotted in Figure 6.

The numerical model showed an accurate prediction of the cracking pattern for the beam strengthened by U-wrap. For Beam B7-UW-250-2, the model shows a crack that propagates behind the CFRP U-wrap and continues propagating towards the support. During testing, this crack is the one causing debonding of the CFRP sheet as shown in Figure 7c. This is numerically illustrated (Figure 11d) via the significant high strains values which exist at the interface (contact) elements between the CFRP sheets and concrete.

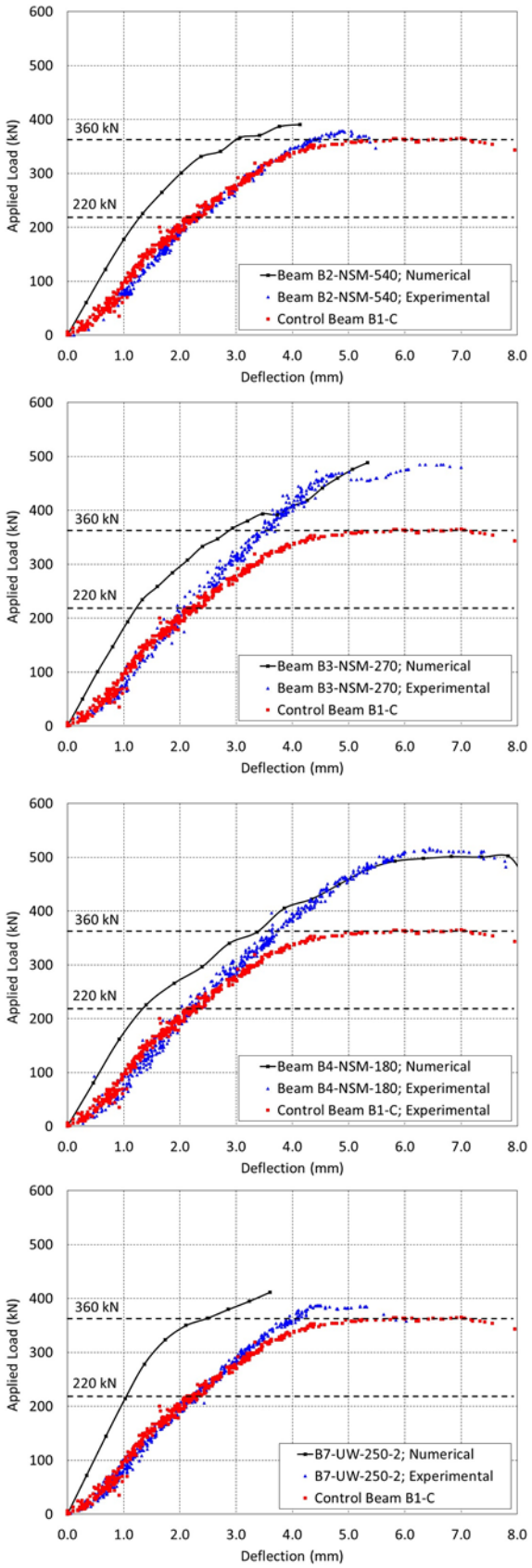

Figure 10. Load-deflection relations obtained numerically and recorded experimentally.

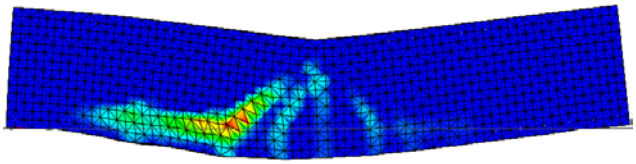

Principal tensile strain

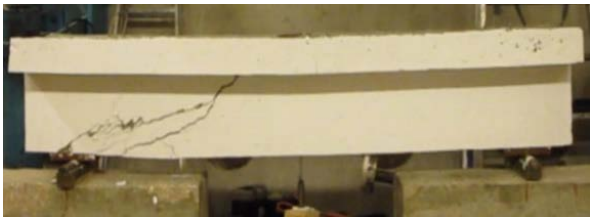

a) Control beam B1-C

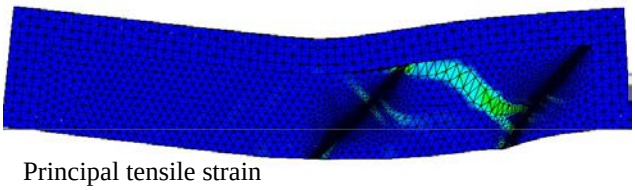

Principal tensile strain

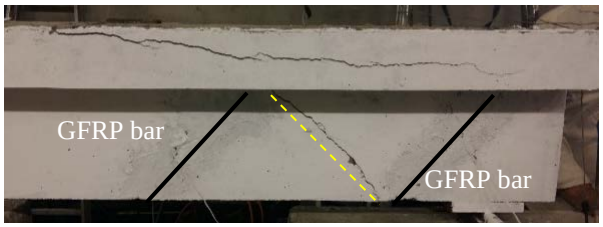

b) NSM strengthened beams with 540 mm bar spacing Beam B2-NSM-540

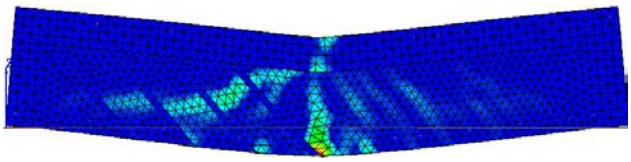

Principal tensile strain

Stresses in steel reinforcement and GFRP bars

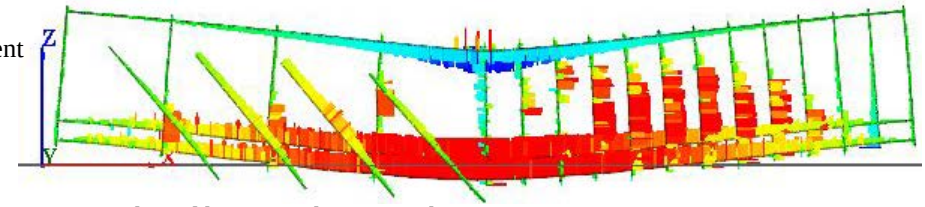

c) NSM strengthened beams with 180 mm bar spacing Beam B4-NSM-180

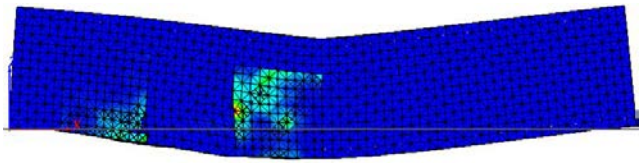

Principal tensile strain

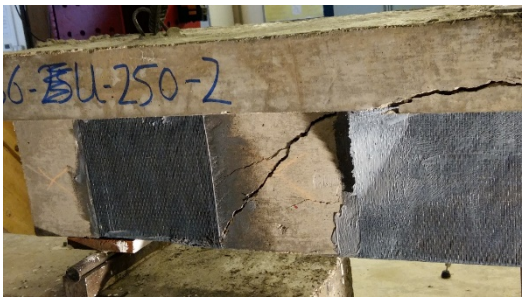

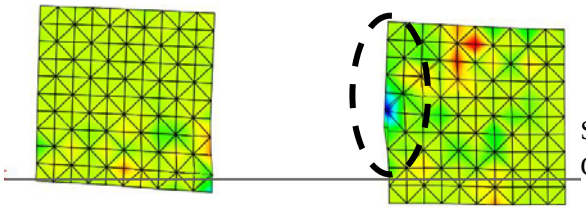

Strains in the interface between CFRP sheets and Concrete

d) U-wrap CFRP sheet strengthened beams Beam B7-UW-250-2

Figure 11. Strains and stresses resulting from the numerical analyses of the beams compared to the cracking pattern experimentally recorded.

6 SHEAR CAPACITY PREDICTION OF STRENGTHENED BEAMS

6.1 *Shear capacity of beams strengthened with NSM FRP bars*

An equation was first proposed by De Lorenzis and Nanni (2001) and adopted by Dias and Barros (2010) to estimate the NSM FRP bar contribution to the shear resistance of an RC beam V_f. With reference to Figure 12, V_f can be given by

$$V_f = \left[2\pi d_b L_{tot-\min} \tau_{bond}\right] \sin\theta \tag{2}$$

where the term in the square brackets is the tensile force that can be developed in the NSM bar, which is resolved vertically to give the V_f, d_b is the diameter of the bar, θ is the angle of inclination of the NSM bars, τ_{bond} is the tensile stress in the NSM bar and $L_{tot\text{-}min}$ is the minimum total length of the FRP bars intercepted by the shear crack which is given by

$$L_{tot-\min} = \sum L_i$$

$$L_i \le L_{\max} = L_{\max} = 0.004 \frac{E_f \frac{\pi}{4} d_f^2}{\pi d_f \tau_{bond}} = 0.001 \frac{E_f d_f}{\tau_{bond}} \tag{3}$$

where L_i is the length of each GFRP bar intercepted by a 45° shear crack as schematically shown in Figure 12 and L_{max} is the effective length of the NSM bar crossed by the crack corresponding to a strain of 0.004; this is a strain limit which is thought to prevent debonding and loss of the aggregate interlock; L_{max} can be estimated by simple force equilibrium as shown in Figure 12.

Dias and Barros [28] used simple geometric relations to estimate $L_{tot\text{-}min}$, which is given with reference to Figure 12 by the following equation:

$$L_{tot-\min} = \sum L_i$$

$$L_i = \begin{cases} for\ i = 1 \ldots \frac{n}{2}: \\ \quad \min\left(\frac{s_f}{\cos\theta + \sin\theta} i\right), L_{\max} \\ for\ i = n + \frac{1}{2} \ldots n: \\ \quad \min\left(L_{net} - \frac{s_f}{\cos\theta + \sin\theta} i\right), L_{\max} \end{cases} \tag{4a}$$

$$L_{net} = L_{bar} - \frac{2c}{\sin\theta}$$

$$L_{eff} = L_{bar} \sin\theta_f - 2c \tag{4b}$$

$$n = \frac{L_{eff}(1 + \cot\theta_f)}{s_f}$$

where s_f is spacing between the NSM bars, E_f is the modulus of elasticity of the NSM FRP bar, c is the concrete cover, n is the anticipated number of bars that will be intersected by the shear crack which is rounded down to the nearest integer, L_{eff} presents the length of the vertical projection of L_{net} and L_{bar} is the length of the FRP bar.

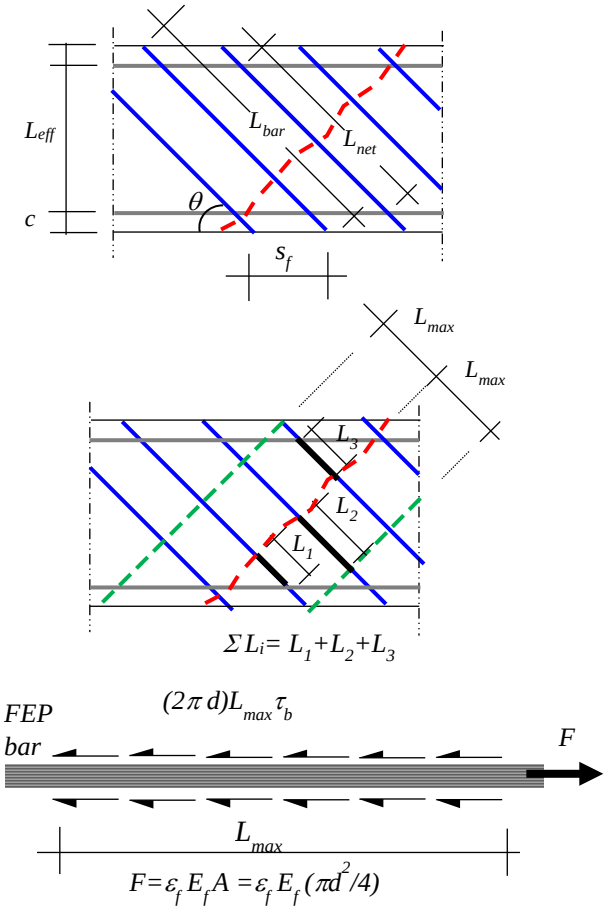

Figure 12. Variables adopted in calculating the contribution of NSM FRP bars to the shear capacity of the beam.

The shear capacity V_n of the NSM FRP bars strengthen beam is then given by

$$V_n = V_c + V_s + V_f \tag{5}$$

where V_c, V_s, and V_f are the contribution to the shear capacity of the concrete, the steel stirrups and the NSM FRP bar, respectively.

For the tested beams strengthened using NSM GFRP bars, the shear capacity was calculated (with reference to Figure 2) by

$$V_{u-\exp} = \frac{P_{u-\exp}}{2} + 0.75w \quad (6)$$

where $P_{u\text{-}exp}$ is the failure load of the beam and w is the beam's own weight. The experimentally recorded shear capacities of the beams are listed in Table 6. The concrete and steel stirrups contribution to the shear capacity of the strengthened beams are considered equal to those recorded experimentally for the control (unstrengthened beams). As such, the NSM FRP bar contribution to shear capacity resulting from the tests can be obtained by subtracting the V_c+V_s from the total shear capacity of the beam for each set; these are also listed in Table 6.

Using Equation 2, the contribution of the NSM FRP bar to the shear capacity V_f is calculated for each beam and listed in Table 6. These values are compared in the same table to their counterparts which were experimentally recorded. The comparison reveals that Equation 2 can predict V_f with a maximum deviation of 13% for the tested beams

Table 6. NSM bar contribution to beams' shear capacity resulting from the experimental program and calculated using Eq 2.

Beam ID	P_u (kN)	$V_{u\text{-}exp}$ (kN)	$(V_c+V_s)_{exp}$ (kN)	$V_{f\text{-}exp}$* (kN)	$V_{f\text{-}Eq.2}$ (kN)	$V_{f\text{-}exp}/V_{f\text{-}Eq.2}$
B1-C	359.6	181.3	181.3	0	-	-
B2-NSM-540	386.9	194.9		13.7	0	-
B3-NSM-270	478.0	240.5		59.2	52.3	1.13
B4-NSM-180	508.7	255.8		74.6	69.0	1.08

* $V_{f\text{-}exp}=V_{u\text{-}exp}-(V_c+V_s)_{exp}$

Equation 2 also correctly predicts the number of NSM FRP bars n intercepted by the shear crack, where the predicted n was 0, 1 and 2 for the 540 mm, 270 mm and 180 mm bars' spacing, respectively; identical to what have been experimentally recorded. Therefore, Equations 2 and 4 are not only able to predict the beam's failure load within a conservative range of 1.08 to 1.13 but they are also able to predict the failure mode of the beams in shear.

6.2 *Shear capacity of beams strengthened with U-wrap CFRP sheets*

For RC beams strengthened in shear using U-wrap FRP sheets, ACI 440.2-08 [29] provides the following equation for predicting the contribution of the laminates to the shear capacity of the beam.

$$V_f = \frac{A_f f_{fe} d_{fv}}{s_f}$$
$$A_f = 2 n t_f w_f \quad (7)$$
$$f_{fe} = \varepsilon_{fe} E_f$$

where A_f is the cross-section area of the CFRP sheet, t_f and w_f are the sheet's thickness and width (Figure 13), respectively, n is the number of plies, f_{fe} is the tensile stress developed in the FRP sheets, ε_{fe} is the effective strain in the sheets, E_f is the elastic modulus of the sheets, d_{fv} is the effective depth of the sheets (depth measured from the tension reinforcement to the edge of the sheet) and s_f is the centerline to centerline spacing between the sheets.

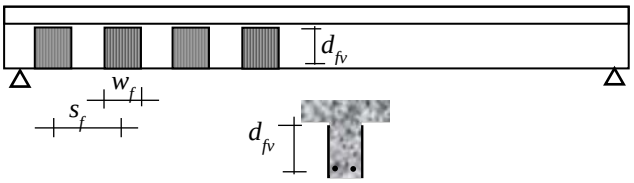

Figure 13. Dimensions and geometry of the U-wrap sheets used to calculate the FRP contribution to the shear capacity of strengthened beams.

The same procedures adopted for calculating the contribution of the NSM FRP bars to the shear capacity of the tested beams are followed herein to predict the CFRP sheets contribution to the beam's shear capacity. These are listed in Table 7 and compared to the values estimated using Equation 7 for beams of tested Sets 5 to 10.

Table 7: Analytical results for U-wrap sets

Beam ID	P_u (kN)	$V_{u\text{-}exp}$ (kN)	$(V_c+V_s)_{exp}$ (kN)	$V_{f\text{-}exp}$* (kN)	$V_{f\text{-}Eq.7}$ (kN)	$V_{f\text{-}exp}/V_{f\text{-}Eq.7}$
B1-C	359.6	181.3	181.3	0	-	-
B5-UW-750-1	472.7	237.8		56.5	50.0	1.13
B6-UW-500-1	469.4	236.2		54.9	50.0	1.10
B7-UW-250-2	387.4	195.2		13.9	25.5	0.54
B8-UW-100-3	463.8	233.4		52.1	15.7	3.32
B10-UW-100-5	442.8	222.9		41.6	30.4	1.37

* $V_{f\text{-}exp}=V_{u\text{-}exp}-(V_c+V_s)_{exp}$

For beams of Sets 5, 6 and 7 which have wide U-wrap CFRP sheets, ACI-440.2R-08 provision (Equation 7) can correctly predict the shear capacity of the 750 mm and 500 mm wide sheets with about 1.1 factor of safety. However, Equation 7 fails to predict the shear capacity for Set 7, which has 250 mm wide sheets with 500 mm centreline to centreline spacing between the sheets: for this set, the crack causing failure propagated in the space between the two

CFRP sheets. Accordingly, this ACI-440.2R-08 provision needs to be revised in terms of adopting a recommended maximum spacing between the sheets such that Equation 7 can safely be applied in design.

For beams of Sets 8 and 10 which have 100 mm width CFRP sheets (Set 9 was excluded due to the premature debonding of the CFRP sheets as explained earlier), Equation 7 predicts the shear capacity of the beams with a factor of safety of 3.3 and 1.37. Thus, Equation 7 deemed to be very conservative for such configuration; it predicts accurate values for closely spaced sheets but deviates from the actual beam capacity by folds for widely spaced sheets. Once again, this confirms the previous conclusion recommending that ACI-440.2R-08 provision needs to adopt a recommended maximum spacing between the sheets.

7 CONCLUSIONS

Two shear strengthening techniques for reinforced concrete beams were experimentally investigated: near-surface mounted GFRP bars and externally bonded U-wrap CFRP sheets. The experimental investigation results were validated using a nonlinear numerical analysis based on the finite element method. Then, the results were used to inspect the validity of the currently available analytical methods for estimating the shear capacity of NSM bars- or FRP laminates-strengthened beams.

Both strengthening techniques proved to be efficient where a shear capacity enhancement of 30% and 40% were achieved for the U-wrap CFRP sheets and NSM bars, respectively. The amount of shear capacity enhancement is significantly affected by the spacing between the NSM bars or the CFRP sheets.

The outcomes of the experimental results were compared to the currently available design equations for both techniques. For the NSM bars, De Lorenzis and Nanni (2001) equation proved to be efficient in predicting the shear capacity of the strengthened beams. However, this equation predicts a continuous increase in the shear capacity by decreasing the spacing between the NSM bars. The experimental investigation reveals that the decrease in the NSM bar spacing is not linearly proportional to the amount of increase in the shear capacity. This fact needs to be addressed in the design equation by setting a limit on the minimum NSM bar spacing.

On the other hand, for the CFRP U-wrap sheets, the ACI 440.2-08 provisions correctly predict the shear capacity of the strengthened beams. However, the code provisions overestimate the shear capacity for wide spacing between the CFRP sheets and underestimate it for narrow one. As such, limiting values for maximum and minimum spacing between the sheets should be implemented in the ACI 440.2-08 provisions.

8 ACKNOWLEDGMENT

The authors acknowledge the support provided by all the technical staff in the AUC Department of Construction Engineering. The in-kind contribution of Schöck ComBar (Germany) for providing the GFRP bars is highly appreciated.

9 REFERENCES

ACI Committee 440. Guide for the design and construction of externally bonded FRP systems for strengthening concrete structure. ACI American Concrete Institute. 2008.

Akroush, N.; Almahallawi, T.; Seif, M.; Sayed-Ahmed, E.Y. CFRP Shear Strengthening of Reinforced Concrete Beams in Zones of Combined Shear and Normal Stresses. Composite Structures, Elsevier, 2017, 162: 47-53.

Alexander, J.G.S.; Cheng, J.J.R. Shear strengthening of small scale concrete beams with carbon fibre reinforced plastic sheets. Proceedings, 1st Structural Specialty Conference, 29 May – 1 June 1996, Edmonton, Alberta, Canada, 1996, pp.167–177.

Araki, N.; Matsuzaki, Y.; Nakano, K.; Kataka, T.; Fukuyama, H. Shear capacity of retrofitted RC members with continuous fibre sheets". Proceedings, non-metallic (FRP) reinforcement for concrete structures, Japan Concrete Institute: Japan, Volume 1, 1997, pp. 512–522.

Bakay, R.; Sayed-Ahmed, E.Y.; Shrive, N.G. Interfacial debonding failure for reinforced concrete beams strengthened with CFRP strips. 2009, Canadian Journal of Civil Engineering, 36(1), 103–121.

Barros, J. A. O.; Dias, S. J. E. Near surface mounted CFRP laminates for shear strengthening of concrete beams. Cement and Concrete Composites, 2006, 28(3), 276-292.

Chaallal, O.; Nollet, M. J.; Perraton, D. Strengthening of reinforced concrete beams with externally bonded fibre reinforced-plastic plates: design guidelines for shear and flexure. Canadian Journal of Civil Engineering, 1998, 25(4), 692–704.

Chen, J.F.; Teng, J.G. Shear capacity of FRP-strengthened RC beams: FRP debonding. Construction and Building Materials, 2003, 17, 27–41.

Collins M.P., Mitchell D. Prestressed concrete structures. Englewood Cliffs (NJ): Prentice-Hall, Inc. 1997.

De Lorenzis, L.; Nanni, A. Shear strengthening of reinforced concrete beams with near-surface mounted fiber-reinforced polymer rods". ACI Structural Journal, 2001, 98(1), 60-68.

Dias, S.J.E.; Barros; J.A.O. Performance of reinforced concrete T beams strengthened in shear with NSM CFRP laminates. Engineering Structures, Elsevier, 2010, 32(2), 373-384.

El-Hacha R.; Riskalla S.H. Near-surface-mounted fiber-reinforced polymer reinforcements for flexural strengthening of concrete structures. ACI Structural Journal, 2004, 101(5): 717-26.

Fanning, P.; Kelly, O. Shear strengthening of reinforced concrete beams: an experimental study using CFRP plates. Proceedings, 8th International Conference on Advanced Composites for Concrete Repair, London, U.K., Part 1, 1999, 7pp.

fib Bulletin 14. Externally bonded FRP reinforcement for RC structures". Technical report by Task Group 9.3 FRP (Fiber reinforced polymer) reinforcement for concrete structures. Féderation Internationale du Béton, fib., 130 p. 2001.

Grace, N.F.; Sayed, G.A.; Soliman, A.K.; Saleh, K.R. Strengthening reinforced concrete beams using fibre reinforced polymer (FRP) laminates". ACI Structural Journal, 1999, 95(5), 865–874.

Hosny, A.A.; Sayed-Ahmed, E.Y.; Abdelrahamn, A.A.; Alhlaby, N.A. Strengthening precast-prestressed hollow core slabs to resist negative moments using CFRP strips: an experimental investigation and a critical review of CSA 806-02. Canadian Journal of Civil Engineering, 2006, 33(8), 955–967.

Hutchinson, R.L.; Rizkalla, S.H. Shear strengthening of AASHTO bridge girders using carbon fibre reinforced polymer sheets. Proceedings, 4th International Symposium on Fibre Reinforced Polymer Reinforcement for Reinforcement Concrete Structures, Michigan, United States, ACI publications SP-188, 1999, pp. 945–956.

Kachlakev, D.I.; Barnes, W.A. Flexural and shear performance of concrete beams strengthened with fibre reinforced polymer laminates. Proceedings, 4th International Symposium on Fibre Reinforced Polymer Reinforcement for Reinforcement Concrete Structures, Michigan, United States, ACI publications SP-188, 1999, pp. 959–971.

Khalifa, A. Shear performance of reinforced concrete beams strengthened with composites, PhD Thesis, Structural Engineering Department, Alexandria University, Egypt. 1999.

Khalifa, A.; Gold, W.J.; Nanni, A.; Aziz, A.M.I. Contribution of externally bonded FRP to shear capacity of RC flexural members. ASCE Journal of Composite for Construction, 1998, 2, 195–202.

Khallifa, A.; Nanni, A. Improving shear capacity of existing RC T-section beams using CFRP composites". Cement and Concrete Composites, 2000, 22, 165–174.

Khalifa, A.; Tumialan, G.; Nanni, A.; Belarbi, A. Shear Strengthening of Continuous RC Beams Using Externally Bonded CFRP Sheets. Proceedings, 4th International Symposium on Fibre Reinforced Polymer Reinforcement for Reinforcement Concrete Structures, Michigan, United States, ACI publications SP-188, 1999, pp. 995-1008.

Nanni A.; Di Ludovico M.; Parretti R. Shear strengthening of a PC bridge girder with NSM CFRP rectangular bars. Advances in Structural Engineering, 2004, 7(4), 97-109.

Petrone, F.; Monti, G. FRP-RC beam in shear: mechanical model and assessment procedure for pseudo-ductile behavior. Polymers, 2014, 6, 2051–2064.

Rizzo A.; De Lorenzis L. Behaviour and capacity of RC beams strengthened in shear with NSM FRP reinforcement". Construction Building Materials, 2009, 23: 1555-1567.

Sayed-Ahmed, E.Y.; Bakay, R.; Shrive, N.G. Bond strength of FRP laminates to concrete: state-of-the-art review. Electronic Journal of Structural Engineering, 2009, 9, 45–61.

Sayed-Ahmed, E.Y.; Riad, A.H.; Shrive, N.G. Flexural Strengthening of Precast Reinforced Concrete Bridge Girders Using Bonded CFRP Strips or External Post-Tensioning. Canadian Journal of Civil Engineering, 2004, 31(3), 499–512.

Sena-Cruz J.M.; Barros J.A.O. Bond between near-surface mounted CFRP laminate strips and concrete in structural strengthening. Journal of Composite for Construction, 2004, 8(6): 519-527.

Teng, J.G.; Chen, J.F.; Smith, S.T.; Lam., L. RC structures strengthened with FRP composites, Hong Kong Polytechnic University, Hong Kong, China, 2000, 134p.

Teng, J.G.; Chen, J.F.; Smith, S.T.; Lam, L. FRP Strengthened RC structures, John Wiley & Sons Ltd., Chichester, UK, 2002, 245p.

Triantafillou, T.C.; Antonopoulos, C.P. Design of concrete flexural members strengthened in shear with FRP. ASCE Journal of Composites for Construction, 2000, 4(4), 198–205.